JOURNAL OF SPACECRAFT AND ROCKETS
Vol. 39, No. 4, July–August 2002

Applications of a Counterflow Drag Reduction Technique in High-Speed Systems

Eswar Josyula,* Mark Pinney,† and William B. Blake‡
U.S. Air Force Research Laboratory, Wright–Patterson Air Force Base, Ohio 45433-7521

Potential applications of a counterflow drag-reduction technique were investigated to assess performance improvements on aerospace vehicles. The motivation for this study was the 30–50% drag reduction achieved by counterflow blowing experiments on hemispherical cylinders at Mach 4 and higher. Exploratory studies indicate that drag improvements by counterflow drag reduction on hemispherical bodies cannot match those of aerodynamically shaped sharp-nosed bodies. Hence, the approach taken in the present study is that for hypersonic Mach numbers: if the nose shape is required to be blunt for considerations other than drag, counterflow blowing can be effective in improving the performance of the system. Although for generic body shapes counterflow blowing is most effective for blunt-nosed bodies, when applied to actual systems, many other factors need to be considered, such as available internal volume and extreme compressed carriage requirements. Depending on the vehicle speed and nose shape, estimated drag reductions of 15–30% were applied to predict the overall performance gains on Space Operations Vehicle, Gun-Launched Rocket, and Pegasus XL configurations. Potential savings in propellant and improvements in burnout velocity and range are reported. For launch systems with high fuel fraction, the payoff with counterflow drag reduction is marginal as the overall effects of aerodynamic drag on performance are small in the upper atmosphere. For the lower fuel fraction vehicle, the Gun Launched Rocket, a range improvement of 7% was achieved for a drag reduction of 30% with 0.3 blunting of nose flying above Mach 3; with greater blunting, however, the volume of fuel cannot compensate for the increase in drag.

Nomenclature

C_D	=	coefficient of drag force
C_{D0}	=	coefficient of drag force, without jet case
d	=	diameter, in.
FN	=	nose fineness ratio
I_{sp}	=	specific impulse, s
M	=	Mach number
m	=	mass, lbm
p_j	=	jet stagnation pressure, psi
p_0	=	stagnation pressure, psi
R	=	range, ft
r	=	radius of hemisphere, in.
S	=	aerodynamic reference area, ft^2
T	=	thrust, lb
u, v, w	=	components of velocity vector
V	=	velocity vector
Vol	=	volume, ft^3
W_p	=	weight of propellant, lb
γ	=	launch attitude, deg
ρ	=	density, lbm/ft^3
ρ_F	=	fuel density, lbm/ft^3

Introduction

THE large wave drag on a vehicle as a result of the increase in entropy across the shock wave surrounding the body in high-speed flight is a serious consideration in its aerodynamic design. The large drag component affects hypersonic vehicles by loss of performance, increased fuel consumption, reduced speed range, and reduced payload carrying capacity. The wave drag reduction, in aerodynamic applications, by either a structural spike or a jet spike on a blunt-nosed body is well known.[1,2] In recent years counterflow jet interaction using a plasma jet has been identified as an important blunt-body-control mechanism for drag reduction across a wide range of Mach numbers.[3] This development led to further studies to understand the underlying physics of counterflow techniques in blunt bodies using argon and airjets as in Refs. 4 and 5 (see Fig. 1). Counterflow drag reduction (CDR) for the purposes of this paper is defined as the injection of a gas from the nose of a vehicle in the upstream direction. This paper explores potential applications of the CDR technique to reduce drag on some existing, near- and far-term systems. The U.S. Air Force Research Laboratory is attempting to answer the following questions: Why CDR? Where did it come from? How can it be used?

Earlier studies utilized structural nose spikes[6] to reduce drag and to improve electromagnetic communications[7] for reentry vehicles; some special application aerospikes were used to improve the effective aerodynamic nose shape (for example, Trident II SLBM).[8] The unsteady nature of the flowfields induced by the physical spike of the 1960s, however, caused severe structural problems,[8] which is a subject of ongoing research even today.[9] Most recently, work[10] has been done using plasma, gas injection, and other "energy" (laser, microwave, etc.) to reduce hypersonic drag, aeroheating loads, and improve electromagnetic communications.

It is not until now, however, that the issue of the integration of the drag-reduction technique into the full system has received attention. The present paper investigates the potential payoff of this drag reduction technique on Pegasus XL, Space Operations Vehicle (SOV), and a Gun-Launched Rocket. To understand the flow physics better and to make realistic assumptions of drag reductions on these systems, the current paper also conducted a computational study of this drag-reduction technique for different freestream Mach numbers and jet pressures for ogive and hemisphere forebody shapes.

The present paper also explores the possibility of CDR in reducing sonic-boom propagation. One of the chief difficulties in sonic-boom reduction is to know what quantity needs to be minimized to make the boom acceptable. A figure of merit (FOM) suggested by Seebass and Argrow[11] is proportional to aircraft's weight divided by the

Presented as Paper 2001-2437 at the 19th Applied Aerodynamics Conference, Anaheim, CA, 11–14 June 2001; received 1 August 2001; revision received 28 December 2001; accepted for publication 18 February 2002.

*Research Aerospace Engineer, Computational Sciences Branch, Air Vehicles Directorate. Associate Fellow AIAA.
†Aerospace Engineer, Aerospace Integration and Demonstration Branch, Air Vehicles Directorate.
‡Aerospace Engineer, Control Theory Optimization Branch, Air Vehicles Directorate. Associate Fellow AIAA.

three-halves power of the length. The lower the FOM, the better it is to reduce the sonic boom. Improvements in the lift-to-drag ratio and the thrust-to-weight ratio can result in sonic-boom reduction for an aircraft with the same range.[11] However, compromise on any of these traditional figures of merit can result in an increase of sonic boom. Earlier concepts in sonic-boom research proposed reduction in sonic boom by blunting the forebody but paid a penalty by an increase in drag. This low-boom high-drag paradox is discussed by Tam et al.[12] in their experiments in reducing sonic boom on newer concepts in the NASA aeroballistic range. The role of CDR in addressing this paradox is presented in the current paper by studying the attenuation of the strong bow shock wave in the near field of the hemispherical body.

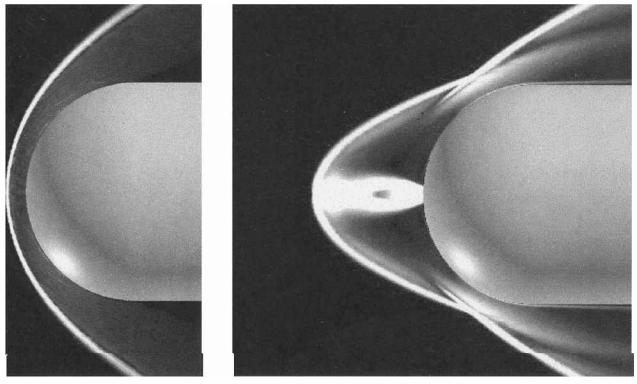

Fig. 1 Change in effective body shape as a result of counterflow jet.

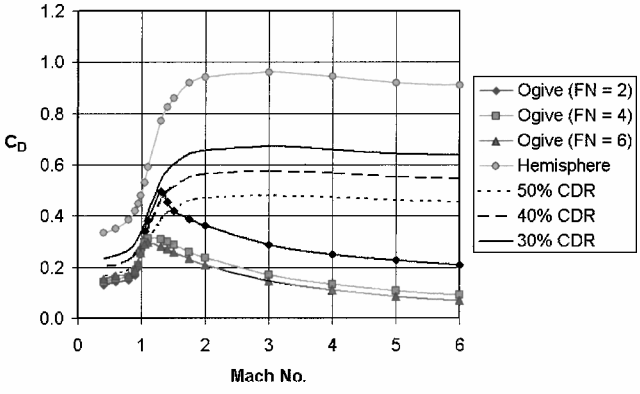

Fig. 2 Typical drag values at various Mach numbers.

The following section provides an overview of the potential applications of CDR. The overview is followed by a description of the flow physics of the counterjet opposing the main stream. The Results and Discussion section presents results of computational studies on generic body shapes and performance assessments on aerospace vehicles.

Overview

From a drag-reduction standpoint counterflow blowing is most suited to systems with a blunt nose at hypersonic speeds. Under these conditions cold-gas CDR might provide a 30–50% (Refs. 4 and 5) nose drag reduction. However, after taking into consideration the percentage contribution of the nose drag to the total drag and the complexity of the potential configuration, the total drag reduction that might be realized could be significantly lower. Furthermore, on pointed nose shapes the nose drag reduction alone can be as small as 5–10% (Ref. 4). In addition, other factors such as available internal volume and integration issues, extreme compressed carriage design requirements (like that of the Trident missile), and critical drag or optimal range requirements need to be looked at for consideration of CDR. Also, CDR would be a candidate technology for aeroheating reduction, although aeroheating is not a consideration in this paper.

Technical Challenges in Aerodynamics

From an aerodynamic perspective the 30–50% drag reduction of a highly blunted nose is not beneficial outside of the transonic region as predicted by the AP93 code,[13] illustrated in Fig. 2. The AP93 code uses a combination of theoretical and empirical techniques to compute the missile aerodynamics in a component-buildup approach. These techniques are the same as used in Missile Datcom,[14] which will be discussed in a later section. In Fig. 2 the drag coefficients C_D of generic nose shapes are compared to a 30, 40, and 50% drag reduction of a 1-ft-diam hemisphere nose. As seen, the aerodynamic shaping alone generally yields lower drag outside of the transonic region.

Technical Challenges at System Level

To illustrate the system integration impact of CDR on the overall drag of a missile system, Fig. 3 shows the nose drag relative to total drag of the vehicle for two typical air-to-air missiles. Calculations were performed based on the AP93 code.[13] One is representative

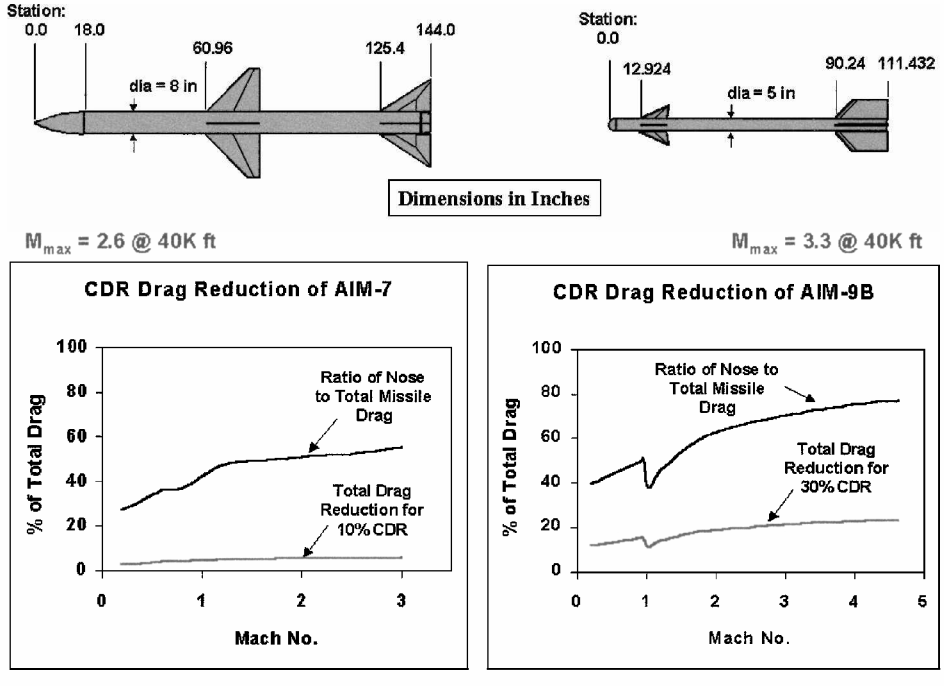

Fig. 3 System level performance.

of a pointed nose configuration (AIM-7) and the other of a blunted nose configuration (AIM-9B). When looking at the contribution of the nose drag to the total configuration drag, one can note how much lower the CDR contributionis to the overall drag levels. Counterflow drag reductions for these configurations were appropriately chosen, based on experimental and computational studies (discussed later), to estimate the total drag reduction on the system. In the case of the pointed nose configuration AIM-7, the CDR contribution was taken as 10% across the Mach-number range, and for the blunted nose configuration, AIM-9B, the CDR contribution was taken as 30%. Therefore, as can be seen from the figure, total drag reductions of 3–5.5% and 12–22% are realized for the pointed and blunted configurations, respectively.

Design and Application Issues

Suitability between nose shape and the Mach-number regime for the application of CDR can be broken down as follows: CDR is most suitable to highly blunted nose shapes. For subsonic flow blunt nose shapes are acceptable from an aerodynamic perspective, and CDR is not applicable. For supersonic flows in the range of $M < 6$, pointed nose shapes are desired from an aerodynamic standpoint, and CDR has minimal impact. However, at hypersonic ($M > 6$) speeds blunt nose shapes are preferred for aeroheating reasons, where CDR has its maximum benefit. CDR is also best suited to systems where the nose drag is a significant percentage of the total vehicle drag.

As already stated, system integration is difficult because of limited available volume in existing vehicles, potential seeker interference, etc. Additionally, the CDR integration issue is further complicated because of the necessity of a source of gas that would be sufficient to achieve the required levels of steady blowing. Inclusion of a gas source involves designing the CDR system with the correct mass flow rate, injection pressure, thermodynamic properties, etc., in harmony with the vehicle flight performance conditions such as Mach-number range, angle-of-attack range, and altitude limits.

All of these factors combined demonstrate the need to balance any potential CDR benefits with existing system design and performance improvement needs.

Potential Applications

The prime objective of this study was to identify potential applications for drag reduction on existing or near-term systems. Potential systems were looked at with respect to their projected initial operational capability (IOC) dates to determine whether they were near- or far-term applications. Existing systems included those that, if not fully operational, contained all of the necessary functional hardware/components and were projected to be operational within the next few years. Near-term systems had IOC dates within the next 5–10 years and far-term systems exceeding 10 years. One application that falls into the unknown category is sonic-boom reduction.

A first-order approximation of the system performance benefits of CDR was conducted on most of these systems, given available generic system information. These results are summarized in Table 1. These results should be viewed as relative comparisons only, not as final system performance benefits. The AIM-7 and AIM-9B were included as reference cases representative of classical air-to-air missiles. Drag-dominant vehicles were considered to be designed for a cruise condition (that is, thrust equal drag) or in a sustained rocket thrust condition. Thrust-dominant vehicles were considered to be accelerating for most of their flight or where the boost portion of the trajectory was dominant. Therefore, for the drag-dominant case the figure of merit was taken as range improvement, and for the thrust-dominant case the figure of merit was delta velocity achieved or pounds of propellant saved. Table 1 gives perfomance improvements in systems with widely different weights and nose diameters. The perfomance improvements are shown as total drag effected on the system for counterflow drag reductions of 10–30% based on experimental and computational studies on generic forebodies. The percent change in the range for the AIM-7 and AIM-9B systems shows the high influence of nose shape on perfomance improvement. Performance improvements on specific systems are discussed later in the Results and Discussion section.

The assumed CDR values used for all estimates were 30% for blunt nose shapes and 10% for pointed nose shapes to simplify the analysis and distinguish between the level of CDR achievable between blunted and pointed nose shape bodies. It must be stressed that the performance benefits shown represent very optimistic levels. The actual benefit levels that would be achievable are dependent on actual CDR system design studies to identify the required amount of gas, CDR system weight, etc.

Flow Physics

This section presents the background research in CDR technique and the complex flow physics associated with it. Interest in reducing the strength of the bow shock wave using airjets began in the late 1950s; the detailed work by Romeo and Sterrett[15] for a Mach 6 helium and argon flow shows the large displacement of the shock and the change in the shock shape. They found that the ratio of the jet total pressure to freestream total pressure necessary to obtain the large displacements depended on the ratio of body diameter to jet-exit diameter and also on the jet-exit Mach number. The maximum amount the shock could be displaced was observed to increase with increasing jet-exit Mach number and also with decreasing ratio of body diameter to jet-exit diameter. For the models investigated, the displacement became very unsteady and fell off sharply as the angle of attack increased. The experimental work by Finley[1] confirmed the earlier observations that the aerodynamic features of a steady flow depend primarily on a jet flow-force coefficient and the Mach number of the jet in its exit plane. The work offered the aerospace community, at the time, a viable technique to reduce drag and provide heat protection on bluff bodies.

A summary of the physics of counterflow jets for blunt bodies discussed in earlier studies[1,16] follows. The counterjet issuing from the body interacts with the supersonic stream causing the bow shock wave to stand away from the surface and takes the form of a new body, which consists of the original body with a protrusion (Fig. 1). The boundary of the protrusion is defined by the interface. The jet separates from an orifice in the forebody, and moves forward to an interface with the mainstream. The fluid from the jet is deflected out and back over the toroidal recirculation region in the jet layer, to a reattachment line (Fig. 4). There is a pressure rise associated with the reattachment of the shear layer. A shear layer is formed on either side of the stream surface, which goes out and back. Fluid is

Table 1 Potential performance benefits summary

System	Initial weight, lb	Fuel fraction	Nose shape	Assumed % CDR	% Total drag	Velocity change, %	% Fuel weight	% Total weight	% Range change
Aim-7	500	0.27	Ogive	10	3–3.5	+0.98	3.50	0.92	+2.8
Aim-9B	197	0.31	Hem	30	12–22	+2.2	7.20	2.20	+13.6
Patriot (PAC 2)	2,200	0.5	~Ogive	10	4.5–6	+0.25	0.22	0.11	——
Patriot (PAC 3)	700	0.51	~Ogive	10	3	+0.41	0.36	0.19	——
Pegasus XL	52,271	0.64[a]	~Blunt	30	8–20	+1.02	0.92	0.58	——
SOV (1sto)	677,000	0.82	~Blunt	30	12–23	+1.47	0.46	0.38	——
SOV (2sto)	1,270,000	0.575[a]	Blunt	30	18–27	+1.4	1.05	0.70	——
THAAD	1,323	0.68	~Ogive	10	3.5–4.5	+1.4	——	——	——
Gun Projectile	110	——	~Ogive	10	5	——	——	——	+4.1

[a]Booster stage.

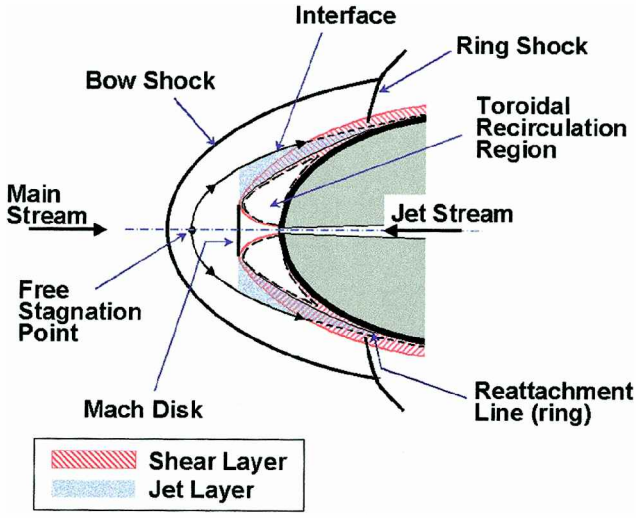

Fig. 4 Flow features of counterflow jet opposing a main stream (adapted from Ref. 1).

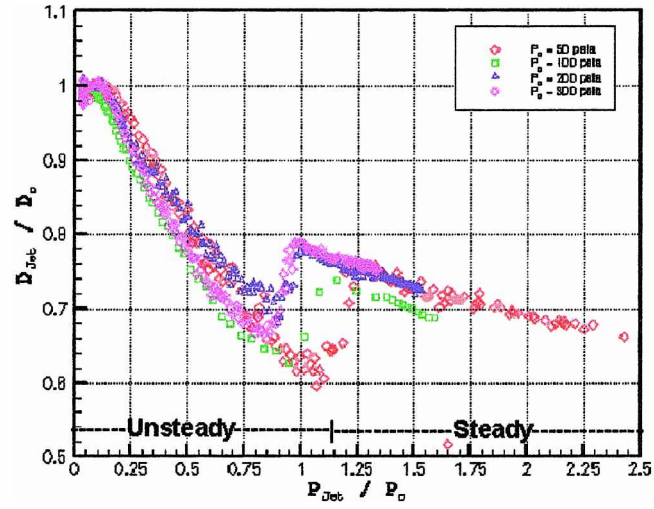

Fig. 5 CDR at various jet pressures (used with permission); experimental study[5] Mach 5.85 flow past hemisphere cylinder.

entrained into the shear layer from the toroidal recirculation region and returned at the reattachment line (ring). The jet layer turns along the body surface and flows downstream.

In a steady flow case both the freestream and the jet come to rest on the axis at a free stagnation point where the pressure is the freestream pitot pressure p_0. As the jet total pressure ratio increases from a value of 1, the bow shock moves forward, and the pressure on the forepart of the body drops. However, there is a critical range of the ratio of the jet pressure p_j to stagnation pressure p_0, given by p_j/p_0, below which the flow is unsteady.[1,5] Above the critical range the flow is mainly steady with a single jet cell terminated by a normal shock.

The highly organized oscillatory fluid motions are sustained by the feedback of upstream pressure propagation through the subsonic recirculating flow region and by a selective amplification of the shear layer. For the lower injection rate the recirculating zone beneath the free-shear layer and the subsonic region immediately downstream of the Mach disk are completely embedded in the supersonic flowfield. The feedback loop from the unstable free-shear layer to the Mach disk is therefore closed. Any perturbation generated by the free-shear layer must propagate through the embedded supersonic domain to influence the Mach disk formation; the amplifiable frequency of the free-shear-layer stability through the feedback loop is capable of achieving a resonance. In the study of Shang et al.,[5] two dominant frequencies were identified at 100 and 449 Hz. When the counterflow jet is generated by a sufficiently high stagnation pressure, a supersonic stream will separate the embedded subsonic domain to break down the feedback loop, resonance ceases, and there is steady motion. The critical pressure varied[5] between a value of 0.8–1.05 for a stagnation pressure range of 50–200 psi for a Mach 5.85 airflow past a 1.5-in.-radius hemisphere nose body of length 11.5 in.

The blunt body with injection results in a lower drag as evidenced by the studies mentioned earlier. The wave drag reduction is derived from both the splitting of a single strong shock into multiple shock waves and replacing the blunt body by a slender displacement. Even though the total pressure rise across the multiple shock waves is identical to that of a single shock, the entropy jump across the multiple wave system is much less. This difference is based on the fact that the entropy increment across each shock wave is proportional to the cubic power of the pressure jump. The drag reduction in the study of Shang et al.[5] for a Mach 5.85 flow was 30–40% depending on the operating stagnation pressure (Fig. 5). Figure 5 shows measured drag force normalized with respect to the no-injection case at different jet and wind-tunnel stagnation conditions. There is variation of drag reduction when the stagnation pressures varied, which can be correlated to density in the atmosphere. Also to be noted is the critical jet pressure above which the flow becomes steady.

Analysis

Missile Datcom[14] was used to estimate the drag characteristics of the vehicles to assess the improvements in their performance characteristics as a result of CDR. Missile Datcom is a widely used engineering-level code that uses the component buildup technique to predict vehicle aerodynamics. Code input consists of body and fin geometry, Mach number, altitude, and angle of attack. At each flight condition the six-body axis force and moment coefficients are provided. Both theoretical and empirical methods are included that encompass the entire speed regime from subsonic to hypersonic. For bodies with blunted noses, supersonic wave drag in Missile Datcom is computed using the modified second-order shock expansion method developed by DeJarnette et al.[17] Fin wave drag is computed using linear supersonic theory.[18] Skin-friction drag for bodies and fins is computed using the method of Van Driest[19] for turbulent boundary layers. An empirical shape factor is included for bodies that applies the flat-plate results to axisymmetric bodies. Base drag is computed using the empirical model developed by Moore et al.[20] The program has been shown to provide excellent agreement with experimental data for a variety of configurations.[21] The code provides a complete breakdown of the individual contributions to drag, ideal for assessing CDR, which primarily affects the nose wave drag.

To determine percentage drag reductions on generic nose shapes, a computational fluid dynamics code was used to perform calculations of the counterflow jet issuing from the nose of the cylindrical bodies having hemispherical and ogive nose shapes. This study was performed to understand the effect of freestream Mach number, jet pressure, and body shapes with a counterflow jet issuing from the nose. The complex self-sustained fluid motion of the counterflow jet issuing from the forebody results in a jet spike bifurcation, as discussed earlier. The detailed fluid dynamics of the jet and the multiple shock-wave structure was computed in the present study by the time-dependent, three-dimensional Navier–Stokes equations. The system of governing equations were solved by an existing implicit unstructured Euler/Navier–Stokes numerical code Cobalt$_{60}$ (Refs. 22 and 23) developed by the U.S. Air Force Research Laboratory. The basic algorithm of Cobalt$_{60}$ is based on the Godunov's Riemann formulation and implicit time stepping to yield second-order spatial and temporal accuracy.[24,25] The numerical procedure was developed as a cell-centered, finite volume code able to accommodate a single-grid system.

The governing partial differential equations are discretized by the fully implicit scheme cast as

$$[3(Q^{n+1} - Q^n) - (Q^n - Q^{n-1})]/2\Delta t + \nabla \cdot F = 0 \qquad (1)$$

where the Q is the independent vector of conserved variables, $Q = (\rho, \rho u, \rho v, \rho w, p)$, and F is the flux vector of the Navier–Stokes equations. The details of this formulation can be found in Ref. 22.

Table 2 Details of cases used in this study

Number	Nose	Mach number	Jet	P_j/P_0
1	Hemisphere	5.85	No	——
2	Hemisphere	5.85	Yes	2.6
3	Hemisphere	5.85	Yes	1.4
4	Hemisphere	4	No	——
5	Hemisphere	4	Yes	2.6
6	Hemisphere	4	Yes	1.4
7	Ogive	3	No	——
8	Ogive	3	Yes	1.4

Table 2 gives the cases computed in the present study. Here are the details of the existing experiment[5] simulated in the present study: nose radius, 1.5 in.; mass flow rate, 1.7 lbm/s; jet mass flow rate, 0.21 lbm/s; stagnation pressure, 100 psi; stagnation temperature, 1100°R; and jet-exit Mach number, 2.84. The cases were selected in an attempt to estimate realistic improvements in performance that can be gained by implementing the CDR technique in real systems.

Conditions of Numerical Simulation

The present study includes CFD computations of an experiment,[5] the details of which are listed in the preceding paragraph. Freestream Mach numbers of 4 and 6 for jet pressure ratios (p_j/p_0) of 1.4 and 2.6 were considered (Table 2).

The other geometry considered in this study is an ogive cylinder, 13 diameters in length. This configuration received considerable attention in some earlier studies,[16,26] which compared various computational algorithms and turbulence models. The nose is given by the equation

$$r/d = -0.002615(x/d)^3 - 0.03986(x/d)^2 + 0.30984(x/d) \quad (2)$$

A freestream Mach number of three was used to compare flow with and without the counterflow jet. In the present study the jet-exit Mach number was kept the same in all cases. The jet pressure, however, was varied, as seen in Table 2. A grid-resolution study was performed to determine the number of cells required to achieve grid-independent solutions. The unstructured grid consisted of a total of 336,313 cells for the hemisphere cylinder and 437,186 cells for the ogive cylinder. Iterative convergence was monitored by examining the integrated forces and moments on the body over several characteristic times based on the minimum time-step size. Convergence was assumed to be achieved when the forces and moments did not change more than 1% between two consecutive solutions of one time unit apart. The L2 norm of the residual was also monitored. A criterion of convergence was met after the normalized residual dropped more than five orders of magnitude.

Boundary Conditions

Because supersonic conditions exist at both the inflow and outflow, freestream conditions were applied at the inflow, and at the outflow flow variables were extrapolated from the interior. Freestream conditions were specified along the far-field boundary. For the body surface no-slip velocity components, zero normal pressure gradient, and an adiabatic wall was used. A source boundary condition consisting of the characteristic-based Riemann invariants was used for the jet issuing from the nose of the forebody; the Riemann-invariants boundary condition fixed the entropy at the inflow boundary. The turbulent closure was achieved by the Spalart–Allmaras one-equation model.[27]

Results and Discussion

The results of the detailed computational study using the Cobalt$_{60}$ code on the hemispherical and and ogive bodies is given next. The improvements in performance characteristics on aerospace vehicles using the Missile Datcom code are presented in a subsequent section.

Results of Computational Study

The Mach 4 flow on a hemispherical cylinder, with and without the counterflow jet, is shown in Fig. 6. The ring shock and the protrusion caused by the counterjet giving the shape of a displaced aerodynamic nose, discussed earlier, is similar to what was observed at Mach 5.85

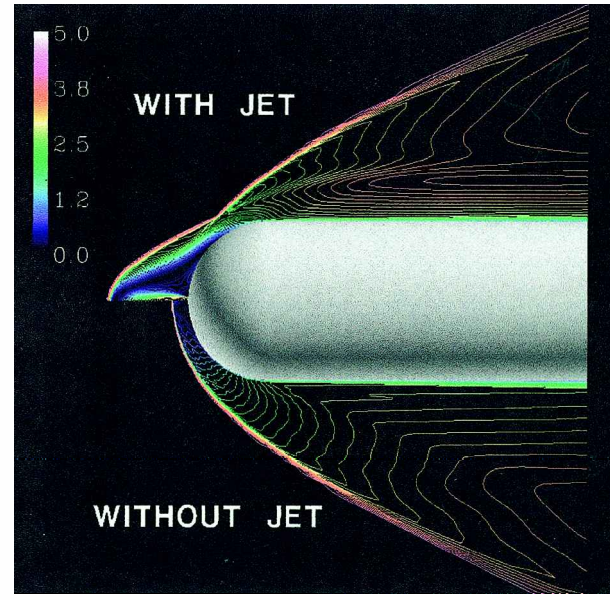

Fig. 6 Comparison of Mach contours for a Mach 4 flow to show effect of counterflow jet, $p_j/p_0 = 1.4$.

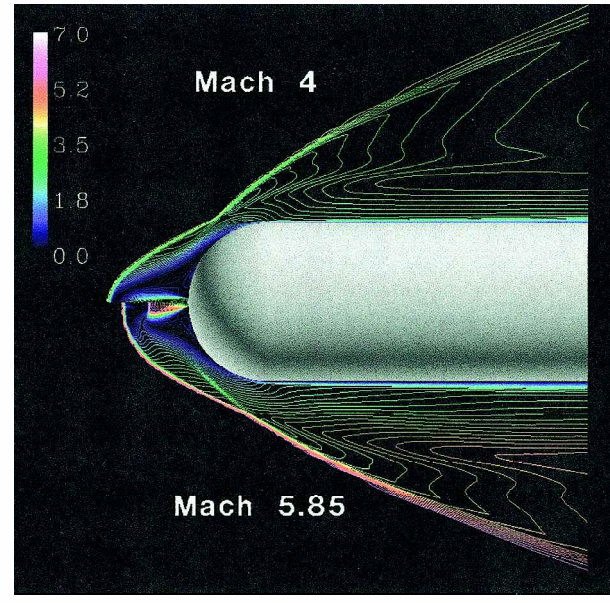

Fig. 7 Comparison of Mach contours to show effect of freestream Mach number on counterflow jet, $p_j/p_0 = 1.4$.

(Ref. 5). The comparison of Mach contours for a Mach 4 and 5.85 flow past a hemisphere cylinder is shown in Fig. 7. The Mach 4 flow clearly shows that the shock moves further away from the body as a result of the counterflow jet, when the jet-exit Mach number is the same in both cases. Because of the greater shock standoff distance for the Mach 4 case, the jet penetration is markedly different for the two cases. This would indicate the need to optimize the jet-exit conditions to get the highest possible drag reduction. The effect of the jet pressure, given by $p_j/p_0 = 1.4$ and 2.6, on a Mach 5.85 flow is shown in Fig. 8. As expected, the shock wave for the higher jet pressure case is further away suggesting a greater reduction in the wave drag component, shown in a later figure. The ring shock location and strength also differs for the two cases.

A Mach 3 flow is depicted for flow past an ogive body with and without a counterjet in Fig. 9. The region of influence of the counterflow jet is limited to the nose section, hence, its limited effect on the shock shape and the reduction in the wave drag component. The very small effect of counterflow jet for ogive nose shapes can also be seen from the correlations presented by Cain and Boyd.[4]

A study of the drag breakdown for different body shapes with counterflow blowing revealed the following. For the flow at the

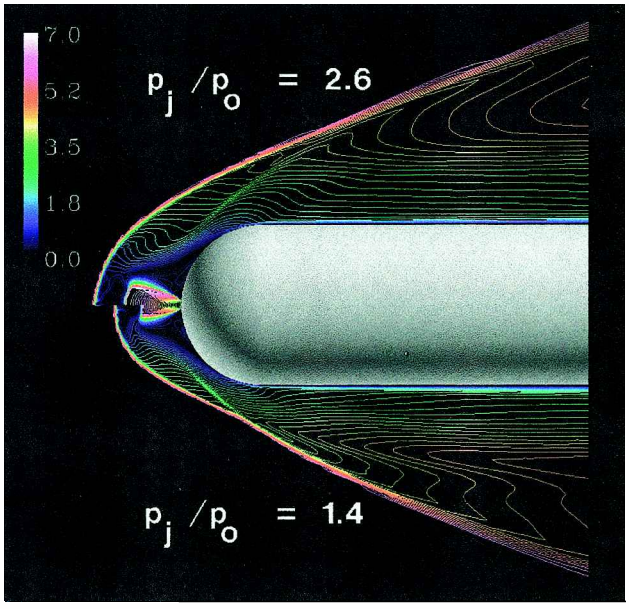

Fig. 8 Comparison of Mach contours for a Mach 5.85 flow to show effect of counterflow jet pressure on flowfield.

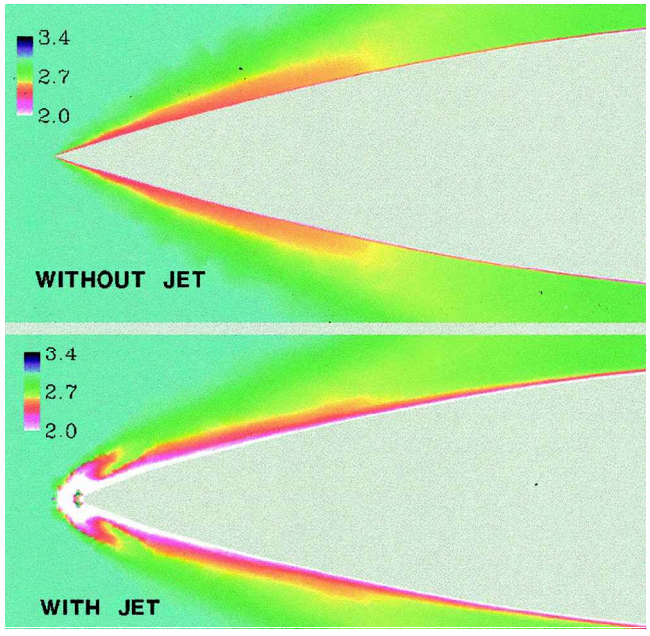

Fig. 9 Comparison of Mach contours for ogive cylinder to show effect of a counterflow jet, $p_j/p_0 = 1.4$; blowup of nose section, 18% total length.

higher Mach number of 5.85 past the hemispherical cylinder as shown in Fig. 7, the total drag is dominated by wave drag (64%) followed by reverse thrust (34%) and negligible viscous drag (2%), whereas for the Mach 3 flow past the ogive cylinder (Fig. 9), the total drag is broken down as wave drag (49%), reverse thrust (16%), and viscous drag (35%). It can be concluded that the CDR technique is effective in vehicles that are wave-drag dominant and not very effective on ogive bodies as a result of the large contribution of viscous drag to the total drag.

A summary chart of the drag prediction as a function of jet pressure is shown in Fig. 10 for the ogive and hemisphere cylinders at different freestream Mach numbers. The drag reduction with counterjet predicted by the present study for a Mach 5.85 flow for a normalized jet pressure of 1.4 is about 30% and is within 10% of the experimental data of Shang et al.[5] The drag prediction at both Mach 4 and 5.85 is lower, with increased jet pressure. Because the jet-exit Mach number is the same for the Mach 4 and 5.85 cases,

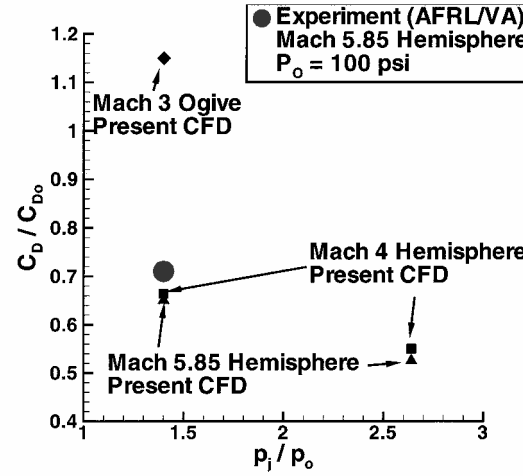

Fig. 10 Comparison of drag reduction caused by counterflow jet.

the drag predictions are close to each other; the drag reduction for the Mach 4 case is slightly higher because of the shock movement further away from the body shown in Fig. 7. However, it is expected that variation in jet-exit Mach numbers with optimum jet penetration will lead to lower drag predictions. For the conditions used in this study, the counterflow jet produces a higher drag for the ogive-nosed body at freestream Mach number of three.

Performance Assessments

This section includes an analysis of several potential applications of CDR and calculations regarding performance improvements. The analysis does not include weight of the CDR system; the predictions as a result could, therefore, be considered as upper bounds. Missile Datcom[14] was used to calculate the drag characteristics of the vehicles.

Pegasus XL

The first applications study of counterflow drag is on the Pegasus XL, which has significant nose bluntness. This is a three-stage, air-launched, solid rocket, 50,000+ -lb system that can boost a 1000+ lb payload into low Earth orbit. Pegasus is dropped from a Lockheed L-1011 transport at 40,000 ft at approximately $M = 0.8$. Following rocket ignition, it enters a 2.5-g pull up while accelerating through the transonic region. It continues to accelerate until staging, which occurs at approximately 150,000 ft at $M = 8$. The performance impact of CDR was determined by computing the reduction in required fuel as a result of reduced drag during the ascent (first-stage motor burn). CDR was assumed to be effective between $M = 3$ and 8, over which the following equation was numerically integrated:

$$\Delta W_p = \frac{1}{I_{\text{sp}}} \int \frac{\rho V^2 S}{2} \Delta C_D \, \mathrm{d}t \tag{3}$$

An I_{sp} of 180 s was assumed. Pegasus has significant nose bluntness, and so a body wave drag reduction of 30% was considered based on experimental and computational studes on generic blunt-nosed forebodies discussed in the preceding section. The counterflow was initiated at $M = 3$ and continued until staging. A plot of the cumulative fuel saved and altitude vs time is shown in Fig. 11. The Missile Datcom representation of the Pegasus XL is shown in the inset of Fig. 11.

Approximately 250 lb of fuel is saved using CDR. This savings represents about 0.8% of the first-stage fuel and 0.5% of the overall gross weight. Only a fraction of this fuel savings (95 lb) can be added to the weight of the upper stages and payload; the rest must be used in the first stage to boost the (now heavier) upper stages. The amount ultimately available for increased payload is less than 10 lb, which is almost negligible and probably less than the weight of the required CDR system.

The vast majority of the first-stage fuel is used to accelerate the vehicle to $M = 8$ and boost it to 150,000 ft. To assess the overall

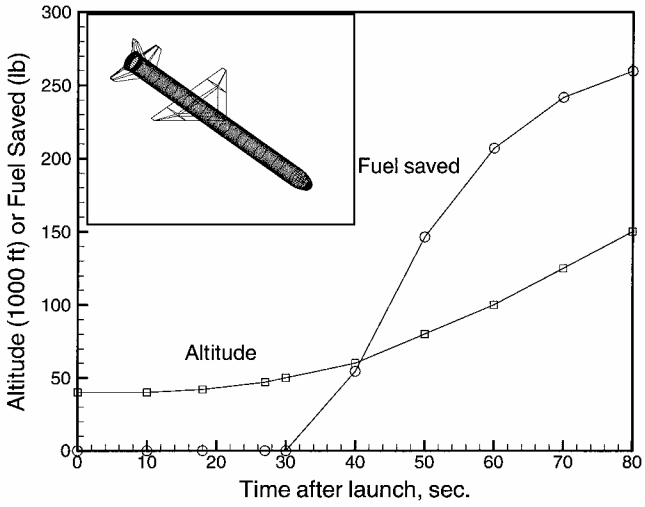

Fig. 11 Fuel savings for Pegasus XL as a result of CDR.

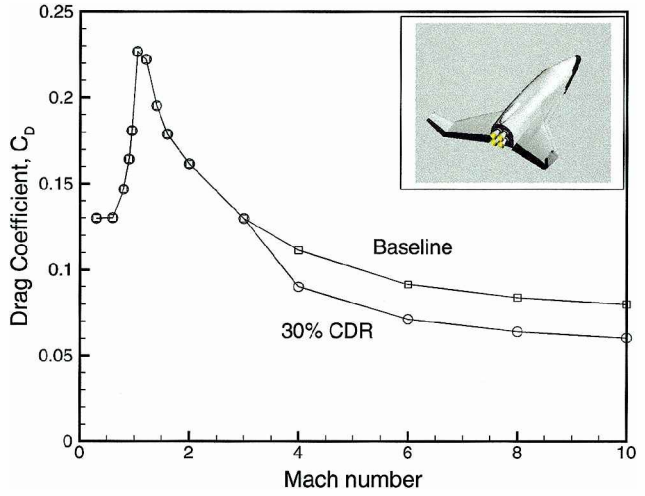

Fig. 12 Drag characteristics of SOV.

impact of aerodynamic drag, Eq. (3) was applied to a trajectory with the total drag reduced to zero. A fuel savings of approximately 6000 lb was attained, indicating that more than 80% of the fuel energy is used for acceleration and boost with less than 20% used to overcome drag. Most of this drag is at transonic or low supersonic Mach numbers where CDR is ineffective. Most of the CDR benefit for this flight profile is at high altitudes (>100,000 ft), where the dynamic pressure is very low so the total drag is much smaller than at lower altitudes.

Space Operations Vehicle

The second application study was performed also on a launch vehicle, SOV (see inset in Fig. 12), but it is different in many respects. The SOV is a single-stage, vertical take-off liquid fuel concept. The drag characteristics of this system are shown in Fig. 12. The counterflow was initiated at $M = 3$ and continued until main engine cutoff (over 200,000-ft altitude). Integrating Eq. (3) resulted in a fuel savings equal to 0.2% of the gross weight. As a fraction of launch weight, the fuel savings is smaller than for the Pegasus XL. Liquid fuel has an I_{sp} about double that of solid fuel, which Eq. (3) shows will reduce the weight savings. Additionally, a ground-launched vehicle must expend significant fuel to reach the equivalent initial condition of an air-launched system. The fraction of fuel savings that can be added to available dry weight is 18% for this vehicle. Because it is a single-stage system, all of this can be applied to the payload to orbit. The system has a payload to lauch weight fraction of 1.8%, so that the increase in available payload is 2%. This increase is relatively small and does not account for the weight of the required CDR system. For launch systems in general, CDR does not appear to have a significant payoff because the high-speed flight takes place in the upper atmosphere where the overall drag levels are small and the bulk of the fuel is used for boost and not to overcome drag.

Gun-Launched Rocket

The next application study is to a gun-launched rocket projectile. The baseline system has an overall fineness ratio of about 10 and a sharp Von Kármán nose shape for minimum wave drag. Deployable fins are used for stability after launch. The assumed CDR application

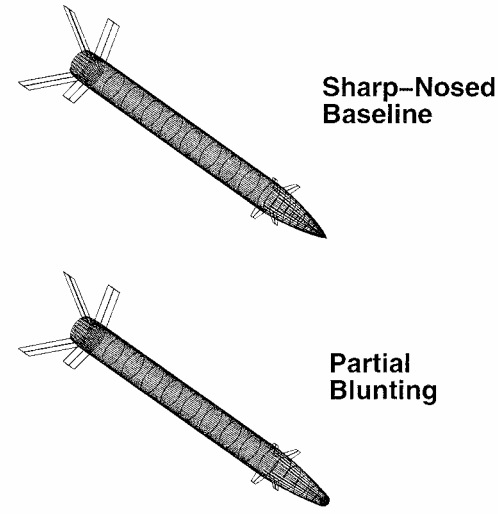

Fig. 13 Missile Datcom representation of sharp-nosed baseline and blunted-nose configuration.

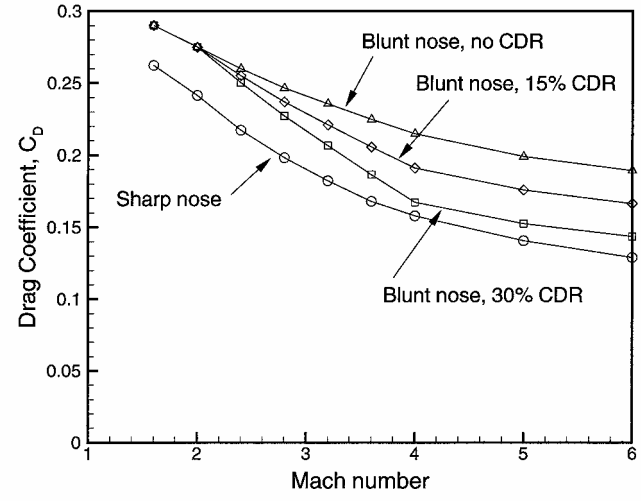

Fig. 14 Drag characteristics.

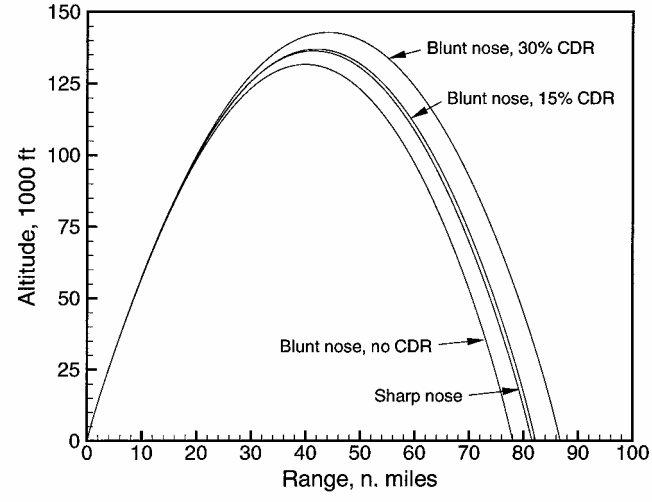

Fig. 15 Flight profiles.

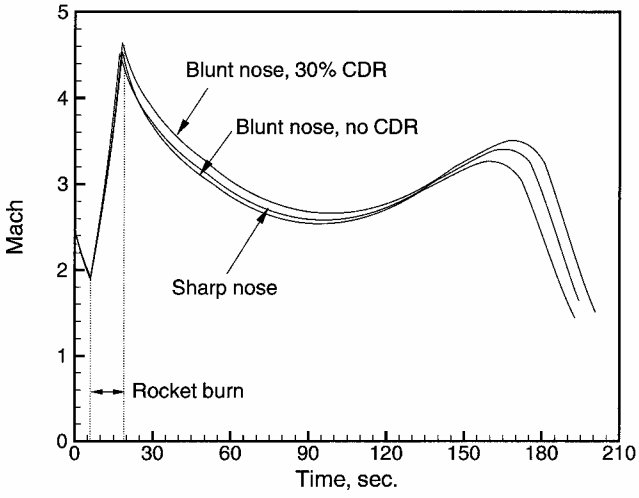

Fig. 16 Mach-number profiles.

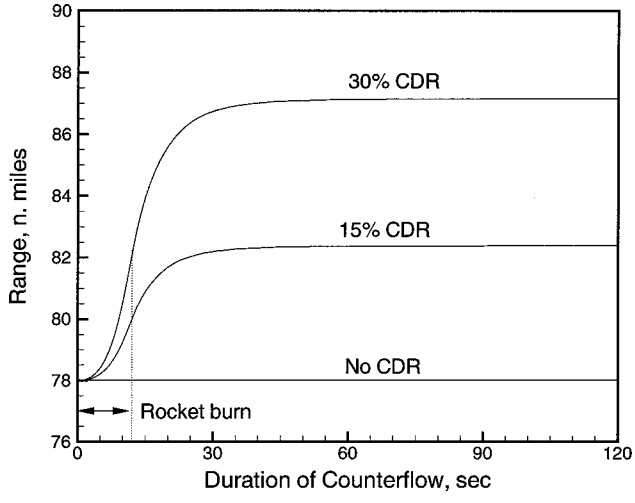

Fig. 17 Effect of duration of CDR.

for this system is to partially blunt an otherwise sharp nose and make use of the added volume for fuel. For this type of application to show a CDR benefit, the volume required for the CDR system itself must not exceed a certain threshold. This threshold can be estimated from the basic rocket range equation for a sustained velocity:

$$R = \frac{2\rho_F g I_{sp} Vol_F}{\rho V S C_D} \tag{4}$$

For a system using CDR by blunting the nose to obtain additional internal volume, this can be rewritten as follows:

$$R = \frac{2\rho_F g I_{sp}(Vol_F + \Delta Vol_F)}{\rho V S(C_D + \Delta C_D)} \tag{5}$$

$$\frac{\Delta Vol_{CDR}}{Vol_N} = \frac{\Delta Vol_{tot}}{Vol_N} - \frac{\Delta Vol_F}{Vol_N} \tag{6}$$

Here, ΔVol_{tot} is the volume obtained from nose blunting, ΔVol_F is the added fuel volume, ΔVol_{CDR} is the volume of the CDR system, Vol_N is the volume of the unblunted nose, and ΔC_D is the change in drag caused by both nose bluntness and CDR. To have a CDR benefit, the following relationship must be satisfied:

$$\frac{\Delta Vol_{CDR}}{Vol_N} < \left(\frac{\Delta Vol_{tot}}{Vol_N} - \frac{\Delta C_D}{C_D}\frac{Vol_F}{Vol_N}\right) \tag{7}$$

This equation shows that the fuel volume of the baseline system as a fraction of the nose volume is a key parameter. It shows that if the fuel fraction (Vol_F/Vol_N) is high benefits from CDR will be small. Hemispherical blunting of a three-caliber sharp nose increases the available volume ($\Delta V_{tot}/V_N$) by more than 80%. However, the drag increases by over 400%, even after accounting for a 30% CDR. To obtain a CDR payoff, the fuel/nose volume ratio would have to be a small fraction of the nose volume, which is very unlikely for a rocket system. More modest nose blunting results in much smaller increases in wave drag. Several nose-bluntness values were studied, and a bluntness ratio of 0.3 was selected. This value increases the nose volume by more than 10% while increasing drag by about 40% (without CDR). It was assumed that the CDR system would occupy 20% of this volume, with the rest allocated to fuel. The effect of added fuel was modeled by a slight increase in burn time instead of an increase in thrust. An I_{sp} of 270 s was assumed.

Missile Datcom representations of the baseline and nose-blunted vehicles are shown in Fig. 13. Drag coefficients were computed

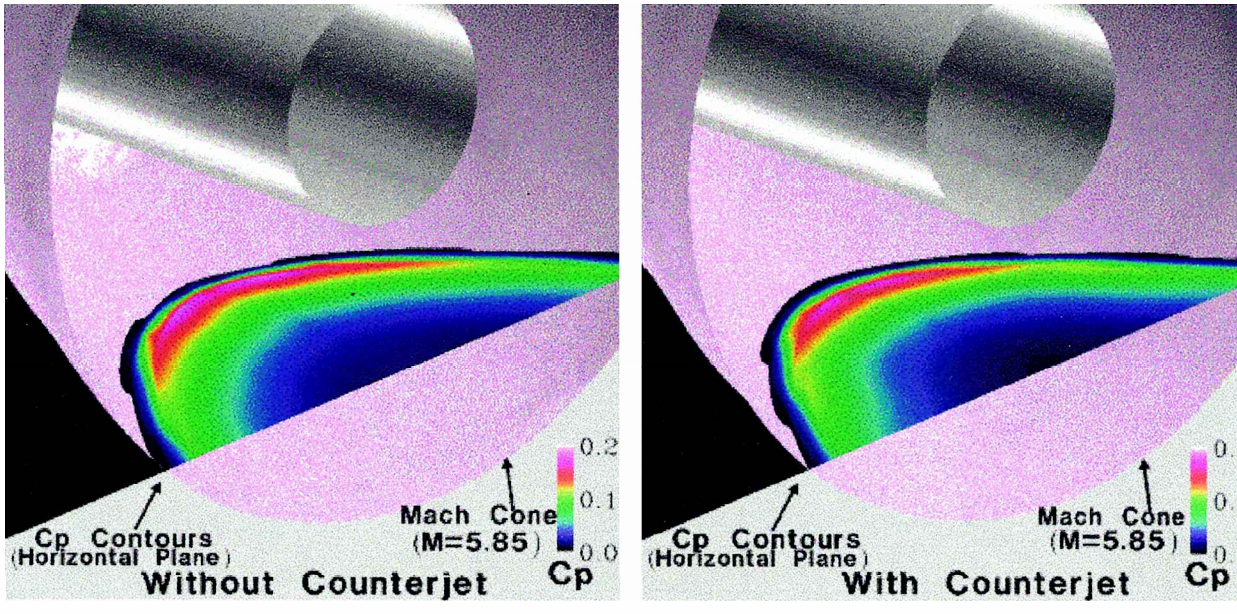

Fig. 18 Pressure intensity on the horizontal plane of Mach cone, with and without jet; looking at aft portion of hemisphere-nose body.

as a function of Mach number and base flow. Base drag increases significantly when the rocket burn is completed. Flight trajectories were computed using a point ballistic model:

$$\dot{u} + (\rho S C_D/2m)(u^2 + w^2)\cos\gamma = (T/m)\cos\gamma \quad (8)$$

$$\dot{w} + (\rho S C_D/2m)(u^2 + w^2)\sin\gamma = (T/m)\sin\gamma - g \quad (9)$$

These equations were integrated numerically with thrust and mass flow varying with time. An initial launch angle (γ_0) of 50 deg was selected for performance comparison. CDR effectiveness was assumed to be zero at $M = 2$ and increase linearly to a prescribed value at $M = 4$. Reductions of 0, 15, and 30% at $M = 4$ were evaluated. A range of values was studied because it is uncertain what the CDR benefit is for partially blunted noses. CDR was activated at rocket ignition (5 s after launch) and remained active for the next 30 s of flight.

The drag characteristics for the cases studied are shown in Fig. 14. Blunting the nose increases drag by about 40% at $M = 4$, with a slightly smaller reduction at lower speeds. CDR of 30% almost reduces the drag to the baseline sharp nose case. Figure 15 shows the computed flight trajectories. A significant portion of the trajectories is over 100,000 ft, where the air is thin and overall drag is small. With no CDR benefit the additional fuel caused by nose bluntness is insufficient to overcome the increased drag, and range decreases by about 5%. With 15% CDR range increases by about 1%. With 30% CDR range increases by about 7%. The Mach-number profiles corresponding to these trajectories are shown in Fig. 16. All are similar. The initial velocity following launch is $M = 2.5$. After a small delay the rocket ignites and accelerates the missile to about $M = 4.5$. The rocket then coasts until impact, with a slight Mach-number increase during initial descent. With CDR an 8-s increase in flight time is attained. The effect of the duration of CDR on overall range is shown in Fig. 17. For reference, the range of the baseline (sharp nose) configuration is 81.5 miles. Almost all of the benefit is attained in the first portion of the flight. During the middle portion of the flight (Fig. 15), the altitude is so high that the overall drag is low. During the latter portion of the flight (Fig. 16), the speed is so low that CDR is ineffective. If CDR is restricted to the rocket burn segment of the flight, about 50% of the maximum possible benefit is achieved. Over 99% of the maximum benefit is achieved within the first 30 s of application of the CDR technique as seen in Fig. 17. There is a knee to the curves indicative of an optimal duration for CDR. Further studies regarding weight and volume requirements for the CDR system are required. Also, the results for this system indicate that further studies are required on CDR for nose bluntness ratios less than 0.5.

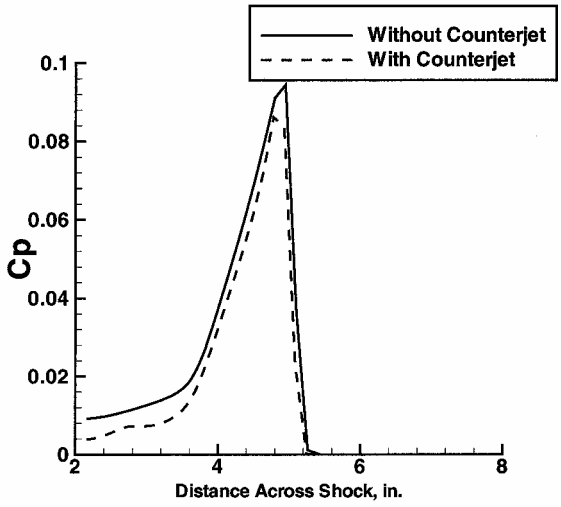

Fig. 19 Comparison of pressure at the outflow of computational domain, Mach 5.85 case.

Other Application: Sonic-Boom Reduction

Exploratory studies were conducted on the effect of counterflow drag reduction in the near-field pressure propagation of the body for possible applications to sonic-boom mitigation of hypersonic vehicles. In these preliminary studies presented in this paper, the effect of counterflow jet on the near-field pressure intensity of the shock wave is shown in Figs. 18 and 19. The Mach 5.85 flow past the hemisphere body with a $p_j/p_0 = 1.4$ is compared to a no-jet case. Figure 18 shows the aft portion of the body where the blunt-body shock wave intersects the Mach cone. Comparison of the pressure contours in the horizontal cutting plane of the Mach cone in Fig. 18 shows that the counterflow jet clearly lowers the pressure intensity, suggesting that the shock-wave attenuation is higher with the injection of a counterflow jet. Figure 19 shows the pressure across the shock wave at the outflow boundary of the computational domain; the pressure with the counterflow jet is about 10% lower. These preliminary studies indicate that in the near field the shock strength reduces as a result of the CDR technique. Further studies are required to predict the effect of CDR on sonic boom intensity in the far field.

Conclusions

The maximum benefit of counterflow blowing for nose drag reduction (CDR of 30–40%) is on highly blunted bodies at high speed ($M > 4$). Most existing blunted-nose vehicles are either subsonic for operational reasons or hypersonic as a result of aeroheating design requirements. Most existing supersonic atmospheric vehicles have slender nose shapes caused by aerodynamic design requirements, where CDR has minimal impact (10% reduction).

System integration is a difficult process based on availability of 1) space or volume for including CDR nozzle and associated piping and 2) counterflow gas to satisfy required jet properties.

Therefore, counterflow blowing is most suited to systems with a blunt nose at hypersonic speeds. Other considerations are 1) available internal volume, 2) extreme compressed carriage requirements, 3) systems with aeroheating problems, and 4) drag critical or optimal range requirements.

For launch systems the payoff for CDR is small because in the upper atmosphere the overall effects of aerodynamic drag on performance are very small. The most promising application for CDR may be for a length-diameter constrained design that operates for significant time at very high speeds in the lower atmosphere. Also, further study on CDR effectiveness is needed for nose-bluntness ratios less than 0.5. By blunting a sharp nose partially, performance benefits and increased fuel volume on the vehicles can be greater than aerodynamic penalties up to a point when the volume of fuel cannot compensate for the increase in drag.

Additional research needs to be conducted to identify the following necessary blowing requirements: 1) cold- or hot-gas requirements based on the available gas source, 2) blowing rates and pressures, 3) nozzle design for optimum jet penetration, and 4) operational Mach number, angle of attack, and altitude limits.

Acknowledgments

Computer resources were provided by the U.S. Department of Defense, High Performance Computing, Major Shared Resource Center at Aeronautical Systems Center, Wright–Patterson Air Force Base, Ohio. The authors wish to acknowledge the support and encouragement by D. Bowers. Computational grids were provided by R. McNutt and K. Wurtzler. The authors are grateful to J. S. Shang for providing the details of the experiment and for many helpful discussions.

References

[1]Finley, P., "The Flow of a Jet From a Body Opposing Supersonic Free Stream," *Journal of Fluid Mechanics*, Vol. 26, No. 2, 1966, pp. 337–370.

[2]Bogdonoff, S., and Vas, I., "Preliminary Investigations of Spiked Bodies at Hypersonic Speeds," *Journal of the Aero/Space Sciences*, Vol. 26, No. 2, 1959, pp. 65–74.

[3]Ganiev, Y. C., Gordeev, V., Kraslinikov, A., Lagutin, V., Otmenikov, V., and Panasenko, A., "Theoretical and Experimental Study of the Possibility of Reducing Aerodynamic Drag by Employing Plasma Injection," AIAA Paper 99-0603, Jan. 1999.

[4]Cain, T., and Boyd, D., "Electrodynamics and the Effect of an Electric Discharge on Cone/Cylinder Drag at Mach 5," AIAA Paper 99-0602, Jan. 1999.

[5]Shang, J., Hayes, J., Wurtzler, K., and Strang, W., "Jet-Spike Bifurcation in High-Speed Flows," *AIAA Journal*, Vol. 39, No. 6, 2001, pp. 1159–1165.

[6]Hutt, G., and Howe, A., "Forward Facing Spike Effects on Bodies of Different Cross Section in Supersonic Flow," *Aeronautical Journal*, Vol. 93, No. 926, 1989, pp. 229–234.

[7]Welsh, W., Jr., "Aerodynamic Spike Experiments on a Sphere in Supersonic Flow," Lab. Operations, Aerospace Corp., TR SAMSO-TR-69-163, El Segundo, CA, March 1969.

[8]Reding, J., Guenther, R., and Richter, B., "Unsteady Aerodynamic Considerations in the Design of a Drag-Reduction Spike," *Journal of Spacecraft and Rockets*, Vol. 14, No. 1, 1977, pp. 54–60.

[9]Mehta, R., "Fluid Dynamics of Self-Sustained Oscillatory Flow over Spiked Blunt-Body at Mach 6.80," AIAA Paper 2000-2225, June 2000.

[10]Toro, P., Nagamatsu, H., Minucci, M., and Myrabo, L., "Experimental Pressure Investigation of a Directed Energy Spike Inlet at Mach 10," AIAA Paper 99-2843, June 1999.

[11]Seebass, R., and Argrow, B., "Sonic Boom Minimization Revisited," AIAA Paper 98-2956, June 1998.

[12]Tam, T., Ruffin, S., Gage, P., Bogdanoff, D., Yates, L., and Morgenstern, J., "Sonic Boom Testing of Artificially Blunted Leading Edge (ABLE) Concepts in the NASA Ames Aeroballistic Range," AIAA Paper 2000-11011, Jan. 2000.

[13]Moore, F. G., Hymer, T., and McInville, R., "An Improved Version of the Naval Surface Warfare Center Aeroprediction Code (AP93)," *Journal of Spacecraft and Rockets*, Vol. 31, No. 5, 1994, pp. 783–791.

[14]Blake, W., "Missile Datcom User's Manual-1997 Fortran 90 Revision," U.S. Air Force Research Lab., TR AFRL-VA-WP-TR-1998-3007, Wright–Patterson AFB, OH, March 1998.

[15]Romeo, D., and Sterrett, J., "Exploratory Investigation of the Effect of a Forward Facing Jet on the Bow Shock of a Blunt Body in a Mach Number 6 Free Stream," NASA TN D-1605, Feb. 1963.

[16]Josyula, E., "Computational Simulation Improvements of Supersonic High-Angle-of-Attack Missile Flows," *Journal of Spacecraft and Rockets*, Vol. 36, No. 1, 1999, pp. 59–66.

[17]DeJarnette, F. R., Ford, C., and Young, D., "Calculation of Pressures on Bodies at Low Angles of Attack in Supersonic Flow," *Journal of Spacecraft and Rockets*, Vol. 17, No. 6, 1980, pp. 529–536.

[18]Hoak, D., and Finck, R., "USAF (United States Air Force) Stability and Control Datcom (Data Compendium)," McDonnell Aircraft Co., TR AFWAL-TR-83-3048, St. Louis, MO, Oct. 1960 (revised 1978).

[19]Van Driest, E., "Turbulent Boundary Layers in Compressible Fluids," *Journal of Aeronautical Science*, Vol. 18, No. 3, 1951, pp. 145–160.

[20]Moore, F. G., Wilcox, F., and Hymer, T., "Base Drag Prediction on Missile Configurations," *Journal of Spacecraft and Rockets*, Vol. 31, No. 5, 1994, pp. 759–765.

[21]Packard, J., and Miller, M., "Assessment of Engineering-Level Codes for Missile Aerodynamic Design and Analysis," AIAA Paper 2000-4590, Aug. 2000.

[22]Strang, W., Tomaro, R., and Grismer, M., "The Defining Methods of Cobalt_{60}," AIAA Paper 99-0786, Jan. 1999.

[23]Tomaro, R., Witzeman, F., and Strang, W., "Simulation of Store Separation for the F/A-18C Using Cobalt_{60}," *Journal of Aircraft*, Vol. 37, No. 3, 2000, pp. 361–367.

[24]Godunov, S., "A Difference Scheme for Numerical Calculation of Discontinuous Solutions of the Equations of Hydrodynamics," *Sbornik Mathematics*, Vol. 47, No. 89, 1959, pp. 271–306.

[25]Tomaro, R., Strang, W., and Sankar, L., "An Implicit Algorithm for Solving Time Dependent Flows on Unstructured Grids," AIAA Paper 97-0333, Jan. 1997.

[26]Sturek, W., Birch, T., Lauzon, M., Housh, C., Manter, J., Josyula, E., and Soni, B., "The Application of CFD to the Prediction of Missile Body Vortices," AIAA Paper 97-0637, Jan. 1997.

[27]Spalart, P., and Allmaras, S., "A One Dimensional Turbulence Model for Aerodynamic Flows," AIAA Paper 92-0439, Jan. 1992.

M. S. Miller
Associate Editor

Color reproductions courtesy of the U.S. Air Force Research Laboratory.